Molecular mechanism regulating myosin and cardiac functions by ELC

Lossie, J., Koehncke, C., Mahmoodzadeh, S., Steffen, W., Canepari, M., Maffei, M., Taube, M., Larcheveque, O., Baumert, P., Haase, H., Bottinelli, R., Regitz-Zagrosek, V., Morano, I.

Biochemical and Biophysical Research Communications
2014 Jul 18 ; 450(1): 464-469
doi: 10.1016/j.bbrc.2014.05.142
Publisher: Elsevier

Molecular mechanism regulating myosin and cardiac functions by ELC

[1]Janine Lossie[*],PhD, [1]Clemens Köhncke[*], MD, [2,3]Shokoufeh Mahmoodzadeh[*], PhD, [4]Walter Steffen, PhD, [5]Monica Canepari, PhD, [5]Manuela Maffei, PhD, [3]Martin Taube, PhD, [3]Oriane Larchevêque, Ms, [6]Philipp Baumert, Ms, [3]Hannelore Haase, PhD, [5,7]Roberto Bottinelli, PhD, [2]Vera Regitz-Zagrosek; PhD, [3,8]Ingo Morano, PhD,

[1]University Medicine Berlin Charité, Experimental and Clinical Research Center (ECRC), Germany; [2]University Medicine Berlin, Charité, Institute of Gender in Medicine, Germany; [3]Max-Delbrueck-Center for Molecular Medicine, Berlin, Germany; [4]Medizinische Hochschule Hannover; Institut fuer Molekular- und Zellphysiologie, Germany; [5]Department of Molecular Medicine and Sport Medicine Research Center, University of Pavia, Italy; [6]Johann Wolfgang Goethe-Universitaet, Institut für Sportwissenschaften, Frankfurt/Main, Germany; [7]Fondazione Salvatore Maugeri, Scientific Institute of Pavia, Pavia, Italy; [8]University Medicine Berlin Charité.

*The first three authors contributed equally to this work

Correspondence to:

Ingo Morano,
Max-Delbrück-Center for Molecular Medicine,
Robert-Roessle-Str. 10,
13125 Berlin,
Germany,
Tel: +49 30 9406 2313,
Fax: +49 30 9406 2277,
e-Mail: imorano@mdc-berlin.de

Abstract

The essential myosin light chain (ELC) is involved in modulation of force generation of myosin motors and cardiac contraction, while its mechanism of action remains elusive. We hypothesized that ELC could modulate myosin stiffness which subsequently determines its force production and cardiac contraction. We therefore generated heterologous transgenic mouse (TgM) strains with cardiomyocyte-specific expression of ELC with human ventricular ELC (hVLC-1; $TgM^{hVLC\text{-}1}$) or E56G-mutated hVLC-1 ($hVLC\text{-}1^{E56G}$; TgM^{E56G}). hVLC-1 or $hVLC\text{-}1^{E56G}$ expression in TgM was around 39% and 41%, respectively of total VLC-1. Laser trap and *in vitro* motility assays showed that stiffness and actin sliding velocity of myosin with hVLC-1 prepared from $TgM^{hVLC\text{-}1}$ (1.67pN/nm and 2.3µm/s, respectively) were significantly higher than myosin with $hVLC\text{-}1^{E56G}$ prepared from TgM^{E56G} (1.25pN/nm and 1.7µm/s, respectively) or myosin with mouse VLC-1 (mVLC-1) prepared from C57/BL6 (1.41 pN/nm and 1.5±0.03 µm/s , respectively). Maximal left ventricular pressure development of isolated perfused hearts *in vitro* prepared from $TgM^{hVLC\text{-}1}$ (80.0mmHg) were significantly higher than hearts from TgM^{E56G} (66.2mmHg) or C57/BL6 (59.3±3.9 mmHg). These findings show that ELCs decreased myosin stiffness, in vitro motility, and thereby cardiac functions in the order hVLC-1 > $hVLC\text{-}1^{E56G}$ ≈ mVLC-1. They also suggest a molecular pathomechanism of cardiomyopathies caused by hVLC-1 mutations.

Key Words: essential myosin light chains; myosin; stiffness; in vitro motility; mutations

Introduction

Two myosin heavy chains (MyHC; 200 kDa each) and four non-covalently linked myosin light chains, two essential myosin light chains and two regulatory light chains (ELC and RLC, resp.: 16-28 kDa), form the native Type II myosin molecule, which is important in the mechanism of muscle contraction

The primary structure of cardiac ELC isoforms presents with an elongated N-terminal (aa 1-46), and a large C-terminal domain (aa 47-≈200) consisting of four helix-loop-helix EF-hand motifs [1,2]. ELCs bind with the utmost lysine-rich N-terminus to actin and with their C-terminal domain to the myosin lever arm (myosin-LA), RLC, and myosin motor domain (myosin-MD) [2,3] and emerged as an important regulatory molecule which determines chemo-mechanical transduction in muscle fibers [3,4,5]. Thus, myosin denuded of ELCs revealed only 1/3 of its normal force generation [5] and reduced *in vitro* actin filament sliding velocity [5,6]. Mutations of MYL3 (accession NM_000258.2), the gene encoding the human VLC-1-Gen, causing familial hypertrophic cardiomyopathy (FHC) disturbed a variety myosin- and cardiac functions in experimental models (for review see [7]), further substantiating the important role of ELC during chemo-mechanical transduction. ELC/myosin binding suggests a structural stabilization of the compliant α-helix of the myosin-LA. This is an important functional aspect since the lever arm is considered to be the elastic element which amplifies the very small conformational changes in the motor domain to a large movement of around 5-10 nm [8]. Association of myosin with ELCs may increase the myosin-LA rigidity and at the same time would power-up force generation per cross-bridge [5,9]. In this study we tested the hypothesis that the association of myosin with different ELC (iso)forms could modulate myosin stiffness and force generation, *in vitro* motility of actin filament sliding, and thus cardiac muscle functions.

To obtain functionally intact myosin and cardiac preparations with weak myosin-binding hVLC-1^{E56G}, we generated heterologous transgenic mouse strains which overexpressed

hVLC-1^{E56G} in the ventricle (TgM^{E56G}). We could show that different ELC isoforms modulate myosin stiffness and force generation and subsequently cardiac contraction. These results could also provide a reasonable pathomechanism explaining the development of FHC by hVLC-1 mutations.

Materials and Methods

Generation of transgenic mice and genotyping

All animal experiments were approved by and conducted in accordance with the guidelines set out by the State Agency for Health and Social Affairs (LaGeSo, Berlin, Germany, G 0178/07).

We generated two transgenic mouse (TgM) models with cardiomyocyte-specific overexpression of the non-mutated human ventricular ELC (hVLC-1) or its E56G mutated form (hVLC-1^{E56G}), i.e. TgM^{hVLC-1} and TgM^{E56G}, respectively (for more details see the Supplemental data).

Cardiac morphology was assessed by echocardiography (Vevo2100, VisualSonics, Toronto, Canada) of 3 month old male TgM^{hVLC-1}, TgM^{E56G} and C57BL/6 mice under light isoflurane (2%) anaesthesia.

For tissue isolation, three months old male transgenic mice were anaesthetized using ketamine hydrochloride (80mg/ml)/xylazine hydrochloride (12mg/ml) administered by i.p.-injection (1mg/kg body weight).

Transcriptome analysis

Total RNA was extracted from ventricles of 3 month old male TgM^{hVLC-1} or TgM^{E56G} (n=4 animals/group) using TRIzol reagent, and transcribed into cDNA with Two-Cycles Target labelling and Control Reagents (Ambion WT Expression Kit and GeneChip WT Terminal Labeling and Hybridization kit, Affymetrix, Santa Clara, CA, USA). Non-pooled microarray experiments were performed with cDNA using GeneChip Mouse Gene 1.0 ST Array (28,853 genes, Affymetrix). For comparison of the expression profiles of TgM^{hVLC-1} with TgM^{E56G}, we considered a False Discovery Rate (FDR-value) of <0.05 and a changed expression level >2.0fold as significant (for more details see Supplemental data).

Transgene incorporation into myosin

We prepared myofibrils according to [10] and ventricular myosin according to [11]. Transgene expression of myosin preparation was evaluated by densitometrical scanning of the Coomassie-stained protein bands and expressed as % of hVLC-1 or hVLC-1^{E56G} of total VLC-1 (transgenic hVLC-1 + endogenous mVLC-1 = 100%) using ImageJ.

Analysis of myosin heavy chain isoenzyme expression

Myosin heavy chain (MyHC) isoenzyme expression pattern was analyzed from ventricular myofibrils by a modified method according to [12]. Briefly, myofibrils were dissolved in 2% SDS and loaded (3 µg/lane) on a SDS-PAGE consisting of a 6% separation gel containing 10% glycerol for 15 h at 50 V const. in the cold room. Gels were stained with Coomassie-blue.

Laser-Trap Analysis

Measurements of the motor mechanics including motor stiffness of single myosins were carried out using an optical trap approach. The optical trapping set-up was based on a Zeiss Axiovert microscope described elsewhere [13]. The positions of the two traps were controlled by electro-optical deflectors (EOD), which were used to move the 2 bead-actin filament-dumbbell relative to the myosin molecule. Actomyosin binding events were detected using the variance-Hidden Markov procedure [14], which gave estimates of the stiffness of each actin-bead linkage and the myosin head. The stiffness of the links was very non-linear and a minimum tension, typically 10 pN, was required for significant noise reduction during myosin binding. To achieve relatively high link stiffness between latex beads and actin filament, we stretched the dumbbell by moving the trapped beads apart at a laser power giving a trap stiffness of about 0.1 pN/nm. The total stiffness along the x-axis of the free dumbbell was then reduced by using a positive feedback system in AC mode as previously described [15]

(for more details see Supplemental data).

In Vitro Motility Assay

Myosin was extracted from glycerinated left ventricular myocardium of TgM^{hVLC-1}, TgM^{E56G}, and C57BL/6 mice and analyzed in the *in vitro* motility assay (IVMA) as described previously [16]. To remove the rigor-like heads from the myosin preparation, after washing out the unbound myosin with bovine serum albumin, the flow cell was washed with two volumes of a solution of 5 µM phalloidin-labeled actin, allowed to incubate for 1–2 min, then washed with 2 volumes of buffer containing 1 mM ATP followed by a wash with experimental buffer (25mM MOPS, 25mM KCl, 4mM $MgCl_2$, 1mM EGTA, 1mM DTT, 200µg/ml glucose oxidase, 36µg/ml catalase, 5mg/ml glucose, and 2mM ATP (pH 7.2 at 25°C)). Actin sliding velocities (Vf) were measured and their distribution characterized according to parametric statistics [16].

Skinned fiber analysis

Demembranated multicellular heart fibers (skinned fibers) were prepared from ventricles of TgM^{hVLC-1} or TgM^{E56G} as described [17]. For mechanical experiments, fibers were dissected into bundles of 150–200 µm diameter and 1-1.5 mm length under a preparation microscope. Fibers were mounted isometrically between a force transducer and a length step generator (Scientific Instruments, Heidelberg) with micro syringes in relaxation solution (25mM imidazol, 10mM ATP, 10mM creatinphosphate, 12.5mM $MgCl_2$, 5mM NaN_3, 1mM DTE, 5mM EGTA, 12.5mM KCl, 380U/ml creatine kinase, pH 7). Sarcomere length was at resting tension (1.95 - 2.0 µm) as detected by laser diffraction analysis. Contraction solution was the same as relaxation solution except that EGTA was substituted by 5mM CaEGTA.

Isolated perfused hearts (Langendorff mode)

Hearts of narcotized animals were rapidly excised and transferred to a dissection dish containing ice-cold modified Krebs-Henseleit buffer containing 118mM NaCl (118.0), 4.7mM KCl, 2mM $CaCl_2$, 2.1mM $MgSO_4$, 24.7mM $NaHCO_3$, 1.2mM KH_2PO_4, 0.06mM EDTA, and 11mM glucose. A 21 gauge stainless steel cannula was inserted into the aorta in the cold buffer dish. Afterwards the hearts were mounted on the Langendorff perfusion rig and retrogradely perfused under constant pressure of 60mmHg at 37°C. Carbogen (5% CO_2, 95% O_2) was delivered to the Krebs-Henseleit buffer to maintain a pH of 7.4. Hearts were electrically stimulated with a coaxial electrode at 414 bpm. To measure left ventricular isovolumetric pressure (LVP) a self-made fluid filled (water) balloon was inserted in the left ventricle. The balloon was connected via a fluid filled tube to a calibrated pressure transducer (APT300, Hugo Sachs Electronics (HSE) Germany). Other parameters were calculated based on the LVP such as maximum rate of pressure increase and pressure decrease (+dLVP/dtmax, −dLVP/dtmax). All data were acquired using the Isoheart software (HSE).

Statistics

Values are means±SEM. Statistical difference between mean values was calculated using Student's t-test for two-tailed unpaired values or 1-way ANOVA and data were considered significant at p-values of < 0.05.

Results and Discussion

Five TgM^{E56G} founders and four TgM^{hVLC-1} founders were genotyped positively, i.e revealed the expected PCR-signal of 989 bp while C57BL/6 mice showed no PCR-signal (Figure 1A). Protein analysis of ventricular myosin obtained from TgM^{hVLC-1}, TgM^{E56G} and C57BL/6 mice by SDS-PAGE showed that the transgenic hVLC-1 forms (25 kDa) were present only in both TgM strains but not in C57BL/6 (Figure 1B). Expression of transgenic hVLC-1 in TgM^{hVLC-1} (n=24) and TgM^{E56G} mice (n=35) were not significantly different (39.1±1.7% and 40.7±1.9%, respectively). We could only detect α-MyHC expression on the myofibrillar protein level in all mouse models investigated (Figure 1C).

Analysis of *in vivo* cardiac morphology and contractile parameters by echocardiography revealed that three month old male TgM^{E56G} developed no cardiac hypertrophy (Supplement data, Table 1). Relative wall thickness and left ventricular mass/body weight ratio remained unchanged in both TgM strains if compared withC57BL/6 (Supplement data, Table 1). In line with our data, a hypertrophic cardiac phenotype could neither be observed in a homologous rabbit model which overexpressed M149V mutated rabbit VLC-1 [18] nor in the homologous TgM model which overexpressed M149V mutated mouse VLC-1 [19]. Likewise, a heterologous TgM model overexpressing A57G mutated hVLC-1 (TgM^{A57G}) did not develop the hypertrophic phenotype [20]. In line, stroke volume, ejection fraction, and fractional shortening were similar in TgM^{E56G}, TgM^{hVLC-1}, and C57BL/6 (Supplement data, Table 1).

We compared the gene expression profiles of the hearts prepared from three months old male TgM^{hVLC-1} or TgM^{E56G} by Affymetrix array experiments (n=4 per group). A total amount of 32 differentially expressed genes (FDR<0.05, expression levels >2fold) were observed between both TgM groups (Supplemental data, Table 2). Hypertrophic marker genes were not differently expressed.

Ventricular single myosin functions TgM^{hVLC-1}, TgM^{E56G} , and C57BL/6, mice were investigated using the laser trap technology. Binding of a single myosin motor to the actin filament resulted in a pronounced reduction of the Brownian movement (reduction of the variance signal) of the dumbbell (Figures 2A-2B). Compared to myosin prepared from C57BL/6 (n=16 motor molecules, 3905 events) the myosin from TgM^{hVLC-1} (n=30 motor molecules, 6789 events) showed a significantly increased motor stiffness, namely from 1.41 ± 0.09 pN/nm to 1.67 ± 0.16 pN/nm. These stiffness values are in general agreement with values obtained from fiber experiments (rabbit psoas) which revealed myosin stiffness of 1.7 pN/nm [21] as well as from optical trap experiments with single myosin molecules (rabbit psoas) demonstrating a stiffness value of 1.79 pN/nm [13]. In contrast, 1.4 pN/nm and 0.4 pN/nm for fast and slow rat skeletal muscle, respectively [22], and 0.7 pN/nm for rabbit skeletal muscle myosin [23] were also reported. The mean stiffness value of myosin with hVLC-1 seems to be underestimated, since it may represent mixed data derived from myosin with mVLC-1 and myosin with hVLC-1 (ca. 40%). Hence, myosin with hVLC-1 ought to have a higher stiffness than myosin with mVLC-1, i.e. ≈2.96 pN/nm in order to be able to increase the observed mean value from 1.41 pN/nm to 1.67 pN/nm. Compared to TgM^{hVLC-1}, ventricular myosin prepared from TgM^{E56G} revealed a significantly ($p<0.001$) reduced mean motor stiffness of 1.25 ± 0.09 pN/nm (n=82 motor molecules, 12847 events) (Figure 2C). On closer examination of myosin with hVLC-1^{E56G}, we noticed two subgroups of motors, one with 0.28 ± 0.04 pN/nm (n=19, 2857 events), significantly lower ($p<0.001$) than myosin from C57BL/6 or TgM^{hVLC-1}, and a second group with 1.60 ± 0.08 pN/nm (n=63, 9990 events), significantly ($p<0.001$) higher compared to myosin from C57BL/6, but not to myosin from TgM^{hVLC-1} (Figure 2B). Binding events with high stiffness produced an apparent working stroke of ~5.1 nm (n=242) and the binding events with low stiffness produced an apparent working stroke of 2.5 nm (n=622). Since $\mathbf{F = \kappa x}$, with x (the working stroke) being 5.1 nm for high-stiffness motors, force generation of single myosin molecules with hVLC-1 and mVLC-1 may be around 16 pN and 7.2

pN, respectively. The species-specific gain-of-function of hVLC-1-myosin compared to mVLC-1-myosin may be based on the different primary sequences of mVLC-1 and hVLC-1 which exert different myosin-LA interaction properties. Taking a working stroke of 2.5 nm of the low-stiffness motors, force generation of single myosin molecules with $hVLC^{E56G}$ may only be around 0.7 pN. There was no distinction in life time of all binding events. Besides the lever arm [24], the converter domain was suggested to represent an alternative element of elastic distortion during force generation [25]. A FHC-related mutation within the converter domain substantially decreased myosin stiffness in fibers [26,27]. 3D-analysis of myosin-S1 suggests close contacts between helix E of ELC with part of the converter domain [2,28], suggesting that ELC could modulate myosin stiffness also via converter domain interaction.

Similar to myosin stiffness and force, *in vitro* actin sliding velocity of ventricular myosin motors with different ELC forms decreased in the order hVLC-1 > $hVLC\text{-}1^{E56G}$ ≈ mVLC-1. Myosin prepared from the ventricles of three months old male $TgM^{hVLC\text{-}1}$ propelled actin filaments significantly ($p<0.001$) faster [velocity of filament transportation (Vf) = 2.3±0.13 µm/s; n=4 animals, 123 filaments] than myosin prepared from TgM^{E56G} (Vf = 1.7±0.07 µm/s; n=5 animals, 98 filaments) (Figure 3). Cardiac myosin prepared from C57BL/6 mice revealed an *in vitro* motility of 1.5±0.03 µm/s (n=3 animals, 89 filaments) which was significantly ($p<0.001$) below the Vf observed with ventricular myosin prepared from $TgM^{hVLC\text{-}1}$ mice (Figure 3A). These reductions could not be due to an increased expression of β-MyHC, which propels actin filaments with a slower velocity than the α-MyHC [11,16]. We could not find any change of the ventricular MyHC isoenzyme expression, neither at the mRNA nor at the protein level.

Rather, *in vitro* actin sliding velocity (***Vf***) decreases if the duty time (***ts***) of XBs increases since $\boldsymbol{Vf = x/ts}$ [29]. Duty time is determined by the ADP release rate from the catalytic site, i.e. ***ts*** decreases if the ADP release rate increases [30]. In fact, similar to the shortening velocity of muscle fibers, ***Vf*** decreases with increasing ADP concentrations [31]. Modulation of the

ADP release rate from the catalytic site by ELC is already suggested by experimental and structural data [32]. The 3D-structures of myosin-S-1 suggest close contacts between helix F and the N-terminal antenna of the ELC to the N-Terminus of the myosin-MD [2,28] [3]. Deletion of the N-terminal aa 1-80 of the myosin-MD destroyed normal ADP release rate of myosin II and could not rescue Dictyostelium myosin-II null cells [33]. We, therefore suggest that the different ELC forms affects *in vitro* actin sliding velocity by modulation of the ADP release rate upon interaction with the N-terminus of the myosin-MD.

Loss-of-function of myosin and reduced *in vitro* velocity of actin sliding suggest deteriorated cardiac contractile parameters which are critically determined by interaction of myosin XBs with actin. Maximal isometric force obtained at maximal calcium activation level (pCa 4.5) of skinned fibers prepared from three months old male TgM^{E56G} was 8.3±1.73 mN/mm^2 (n=10 fibers), i.e. significantly ($p<0.05$) lower than the force obtained from $TgM^{hVLC\text{-}1}$ (13.9±1.5 mN/mm^2 ; n=9 fibers; Figure 3B)). Calcium sensitivities expressed as pCa50 calculated from the tension/pCa curves of fibers prepared from TgM^{E56G} and $TgM^{hVLC\text{-}1}$ was similar (5.44 and 5.41, respectively). Accordingly, TgM^{E56G} and $TgM^{hVLC\text{-}1}$ fibers had similar Hill coefficient (3.5 and 3.2, respectively). The reduced force generation upon expression of hVLC-1^{E56G} is in agreement with a recent work showing that force of skinned heart fibers obtained from TgM^{A57G} decreased [34]. This predicts a "loss of function" of myosin with hVLC-1^{A57G} similar to the myosin with hVLC-1^{E56G} investigated herein and, therefore decreased stiffness. By contrast myosin stiffness of TgM^{A57G} rose [20], indicating a "gain of function" of myosin with hVLC-1^{A57G}. The reason for this discrepancy is yet unknown.

In addition, we investigated *in vitro* contractility of electrically paced isolated perfused hearts in the Langendorff-mode of TgM^{E56G}, $TgM^{hVLC\text{-}1}$ and C57BL/6. Isovolumetric pressure development of left ventricles (LVP) from hearts of TgM^{E56G} (n=10) was 66.2±4.2 mmHg. This was significantly lower compared to LVP of $TgM^{hVLC\text{-}1}$ (80.0±4.6 mmHg; n=9) (Figure 4A). In addition, TgM^{E56G} revealed a significantly reduced maximal rate of isovolumetric pressure

development (LVP_{dtmax} 2982.9±194 mmHg/sec) compared with TgM^{hVLC-1} (LVP_{dtmax} 3613.2±144 mmHg/sec) (Figure 4B) and significantly lower maximal rate of isovolumetric relaxation ($-LVP_{dtmax}$) compared with TgM^{hVLC-1} ($-LVP_{dtmax}$ -1678.2±140 mmHg/sec vs. $-LVP_{dtmax}$ -2465.1±152 mmHg/sec) (Figure 4C). Interestingly, C57BL/6 mice (n=9) revealed *in vitro* contractility parameters significantly lower than the levels observed in TgM^{hVLC-1}, i.e. LVP (59.3±3.9 mmHg), LVP_{dtmax} (2453.4±183 mmHg/sec) and $-LVP_{dtmax}$ (-1553.2±138 mmHg/sec) (Figures 4A-4C). Coronary flow of isolated perfused hearts was similar among all three groups (2.1±0.1, 1.9±0.3, and 2.2±0.4 ml/min in TgM^{hVLC-1}, TgM^{E56G} and C57BL/6, respectively.

The deleterious effects of the E56G mutated hVLC-1 on myosin and cardiac functions described herein may represent a valuable molecular pathomechanism provoking the development of FHC upon hVLC-1 mutations. Those mutations may weaken the myosin-LA affinity, reduce stiffness and unitary force generation of the single myosin molecule, slow down actin filament sliding velocity, and depress cardiac performance. The resulting cardiac hypocontractility could then activate hypertrophic pathways leading to the FHC phenotype [35].

Taken together, we provide a molecular mechanism which could explain the physiological regulation of myosin force generation by ELC forms, namely via distinct myosin-LA affinity which may modulate myosin stiffness and, therefore myosin and cardiac functions.

Acknowledgements

We gratefully acknowledge Petra Sakel, Petra Domaing and Steffen Lutter for technical assistance. This work was supported by DFG GK 754 to J.L. and I.M; DFG STE 1697/2 to W.S. and the German Center for Cardiovascular Research (DZHK) to VRZ.

References

[1] E.M. Aydt, G. Wolff, I. Morano, Molecular modeling of the myosin-S1(A1) isoform, J Struct Biol 159 (2007) 158-163.
[2] I. Rayment, H.M. Holden, M. Whittaker, et al., Structure of the actin-myosin complex and its implications for muscle contraction, Science 261 (1993) 58-65.
[3] S. Lowey, L.D. Saraswat, H. Liu, et al., Evidence for an interaction between the SH3 domain and the N-terminal extension of the essential light chain in class II myosins, J Mol Biol 371 (2007) 902-913.
[4] R. Bottinelli, R. Betto, S. Schiaffino, et al., Unloaded shortening velocity and myosin heavy chain and alkali light chain isoform composition in rat skeletal muscle fibres, J Physiol 478 (Pt 2) (1994) 341-349.
[5] P. VanBuren, G.S. Waller, D.E. Harris, et al., The essential light chain is required for full force production by skeletal muscle myosin, Proc Natl Acad Sci U S A 91 (1994) 12403-12407.
[6] S. Lowey, G.S. Waller, K.M. Trybus, Skeletal muscle myosin light chains are essential for physiological speeds of shortening, Nature 365 (1993) 454-456.
[7] O.M. Hernandez, M. Jones, G. Guzman, et al., Myosin essential light chain in health and disease, Am J Physiol Heart Circ Physiol 292 (2007) H1643-1654.
[8] G. Piazzesi, M. Reconditi, M. Linari, et al., Skeletal muscle performance determined by modulation of number of myosin motors rather than motor force or stroke size, Cell 131 (2007) 784-795.
[9] J. Howard, J.A. Spudich, Is the lever arm of myosin a molecular elastic element?, Proc Natl Acad Sci U S A 93 (1996) 4462-4464.
[10] R.J. Solaro, D.C. Pang, F.N. Briggs, The purification of cardiac myofibrils with Triton X-100, Biochim Biophys Acta 245 (1971) 259-262.
[11] M. Canepari, R. Rossi, M.A. Pellegrino, et al., Speeds of actin translocation in vitro by myosins extracted from single rat muscle fibres of different types, Exp Physiol 84 (1999) 803-806.
[12] U. Carraro, C. Catani, A sensitive SDS-PAGE method separating myosin heavy chain isoforms of rat skeletal muscles reveals the heterogeneous nature of the embryonic myosin, Biochem Biophys Res Commun 116 (1983) 793-802.
[13] A. Lewalle, W. Steffen, O. Stevenson, et al., Single-molecule measurement of the stiffness of the rigor myosin head, Biophys J 94 (2008) 2160-2169.
[14] D.A. Smith, W. Steffen, R.M. Simmons, et al., Hidden-Markov methods for the analysis of single-molecule actomyosin displacement data: the variance-Hidden-Markov method, Biophys J 81 (2001) 2795-2816.
[15] W. Steffen, D. Smith, R. Simmons, et al., Mapping the actin filament with myosin, Proc Natl Acad Sci U S A 98 (2001) 14949-14954.
[16] M. Canepari, R. Rossi, M.A. Pellegrino, et al., Functional diversity between orthologous myosins with minimal sequence diversity, J Muscle Res Cell Motil 21 (2000) 375-382.
[17] I. Morano, F. Hofmann, M. Zimmer, et al., The influence of P-light chain phosphorylation by myosin light chain kinase on the calcium sensitivity of chemically skinned heart fibres, FEBS Lett 189 (1985) 221-224.
[18] J. James, Y. Zhang, K. Wright, et al., Transgenic rabbits expressing mutant essential light chain do not develop hypertrophic cardiomyopathy, J Mol Cell Cardiol 34 (2002) 873-882.
[19] A. Sanbe, D. Nelson, J. Gulick, et al., In vivo analysis of an essential myosin light chain mutation linked to familial hypertrophic cardiomyopathy, Circ Res 87 (2000) 296-302.

[20] P. Muthu, L. Wang, C.C. Yuan, et al., Structural and functional aspects of the myosin essential light chain in cardiac muscle contraction, Faseb J 25 (2011) 4394-4405.
[21] M. Linari, M. Caremani, C. Piperio, et al., Stiffness and fraction of Myosin motors responsible for active force in permeabilized muscle fibers from rabbit psoas, Biophys J 92 (2007) 2476-2490.
[22] M. Capitanio, M. Canepari, P. Cacciafesta, et al., Two independent mechanical events in the interaction cycle of skeletal muscle myosin with actin, Proc Natl Acad Sci U S A 103 (2006) 87-92.
[23] C. Veigel, M.L. Bartoo, D.C. White, et al., The stiffness of rabbit skeletal actomyosin cross-bridges determined with an optical tweezers transducer, Biophys J 75 (1998) 1424-1438.
[24] T.Q. Uyeda, P.D. Abramson, J.A. Spudich, The neck region of the myosin motor domain acts as a lever arm to generate movement, Proc Natl Acad Sci U S A 93 (1996) 4459-4464.
[25] I. Dobbie, M. Linari, G. Piazzesi, et al., Elastic bending and active tilting of myosin heads during muscle contraction, Nature 396 (1998) 383-387.
[26] J. Kohler, G. Winkler, I. Schulte, et al., Mutation of the myosin converter domain alters cross-bridge elasticity, Proc Natl Acad Sci U S A 99 (2002) 3557-3562.
[27] B. Seebohm, F. Matinmehr, J. Kohler, et al., Cardiomyopathy mutations reveal variable region of myosin converter as major element of cross-bridge compliance, Biophys J 97 (2009) 806-824.
[28] R.A. Milligan, Protein-protein interactions in the rigor actomyosin complex, Proc Natl Acad Sci U S A 93 (1996) 21-26.
[29] T.Q. Uyeda, S.J. Kron, J.A. Spudich, Myosin step size. Estimation from slow sliding movement of actin over low densities of heavy meromyosin, J Mol Biol 214 (1990) 699-710.
[30] R.F. Siemankowski, M.O. Wiseman, H.D. White, ADP dissociation from actomyosin subfragment 1 is sufficiently slow to limit the unloaded shortening velocity in vertebrate muscle, Proc Natl Acad Sci U S A 82 (1985) 658-662.
[31] E. Homsher, F. Wang, J.R. Sellers, Factors affecting movement of F-actin filaments propelled by skeletal muscle heavy meromyosin, Am J Physiol 262 (1992) C714-723.
[32] J. Borejdo, D.S. Ushakov, R. Moreland, et al., The power stroke causes changes in the orientation and mobility of the termini of essential light chain 1 of myosin, Biochemistry 40 (2001) 3796-3803.
[33] S. Fujita-Becker, G. Tsiavaliaris, R. Ohkura, et al., Functional characterization of the N-terminal region of myosin-2, J Biol Chem 281 (2006) 36102-36109.
[34] K. Kazmierczak, E.C. Paulino, W. Huang, et al., Discrete effects of A57G-myosin essential light chain mutation associated with familial hypertrophic cardiomyopathy, Am J Physiol Heart Circ Physiol 305 (2013) H575-589.
[35] H. Ashrafian, C. Redwood, E. Blair, et al., Hypertrophic cardiomyopathy:a paradigm for myocardial energy depletion, Trends Genet 19 (2003) 263-268.

Figure Legends

Figure 1: Generation and characterization of transgenic mouse lines

Genomic DNA (ear biopsies) of TgMhVLC-1, TgME56G were used for transgene-specific PCR yielding a fragment of 989 bp. Construct containing hVLC-1 gene and genomic DNA obtained from C57BL/6 were used as positive and negative controls. B) SDS-PAGE (12%) of purified ventricular myosin (1-2 µg/lane) of TgM^{hVLC-1} (Lane 1), TgM^{E56G} (Lane 2), and C57BL/6 mice (Lane 3); RLC: regulatory myosin light chain. C) Analysis of MyHC isoenzyme expression in the myofibrils of left ventricles of male TgM^{hVLC-1}, TgM^{E56G}, and C57BL/6. A fetal mouse ventricle with both α- and β-used to identify MyHC isoenzymes.

Figure 2: Laser trap analysis

A) Representative displacement (top) and variance (bottom) records of binding events to actin-dumbbell of ventricular myosin of TgM^{hVLC-1}. Only binding events with high motor stiffness could be observed (cf. Figure 2C). B) Representative displacement (top) and variance (bottom) records of two types of binding events to actin-dumbbell observed with ventricular myosin of TgM^{E56G}. Please note, that myosin motors with both high (hash mark) and low (asterisks) stiffness events in the same recording were rare observations (3 motors out of a total of 82 motors). C) Motor stiffness of myosin purified from ventricles of 3 months old male C57BL/6, TgM^{hVLC-1}, or TgM^{E56G} using the variance/co-variance model.26 Values are means ± SEM. Data were corrected to compensate for lower frequency (10 kHz) recordings40 , ***$p<0.001$.

Figure 3: In vitro motility assay and Skinned fiber analysis

A) Velocities of actin filaments (Vf) sliding of myosin purified from ventricles of 3 months old male C57BL/6 (3 animals, 123 actin filaments), TgM^{hVLC-1} (5 animals, 98 actin filaments) or TgM^{E56G} (4 animals, 60 actin filaments). B) Isometric force generation expressed in

mN/mm2 cross-section of skinned fibers prepared from cardiac ventricles of 3 months old male TgM^{hVLC-1} (9 fibers) or TgM^{E56G} (10 fibers). Values are means ± SEM; *p< 0.05, ***p< 0.001.

Figure 4: Isolated perfused heart (Langendorff) measurements

A) Maximal left ventricular isovolumetric pressure developments (LVP in mmHg) of TgM^{hVLC-1} (n=10), TgM^{E56G} (n=9) and C57BL/6 (n=9). B) Maximal rates of left ventricular isovolumetric pressure development (LVP/dt max. in mmHg/s). C) Maximal relaxation rates of left ventricular isovolumetric pressure (-LVP/dt max. in mmHg/s). Values are expressed as means ± SEM, *p < 0.05, **p < 0.01, ***p< 0.001.

Figure 1

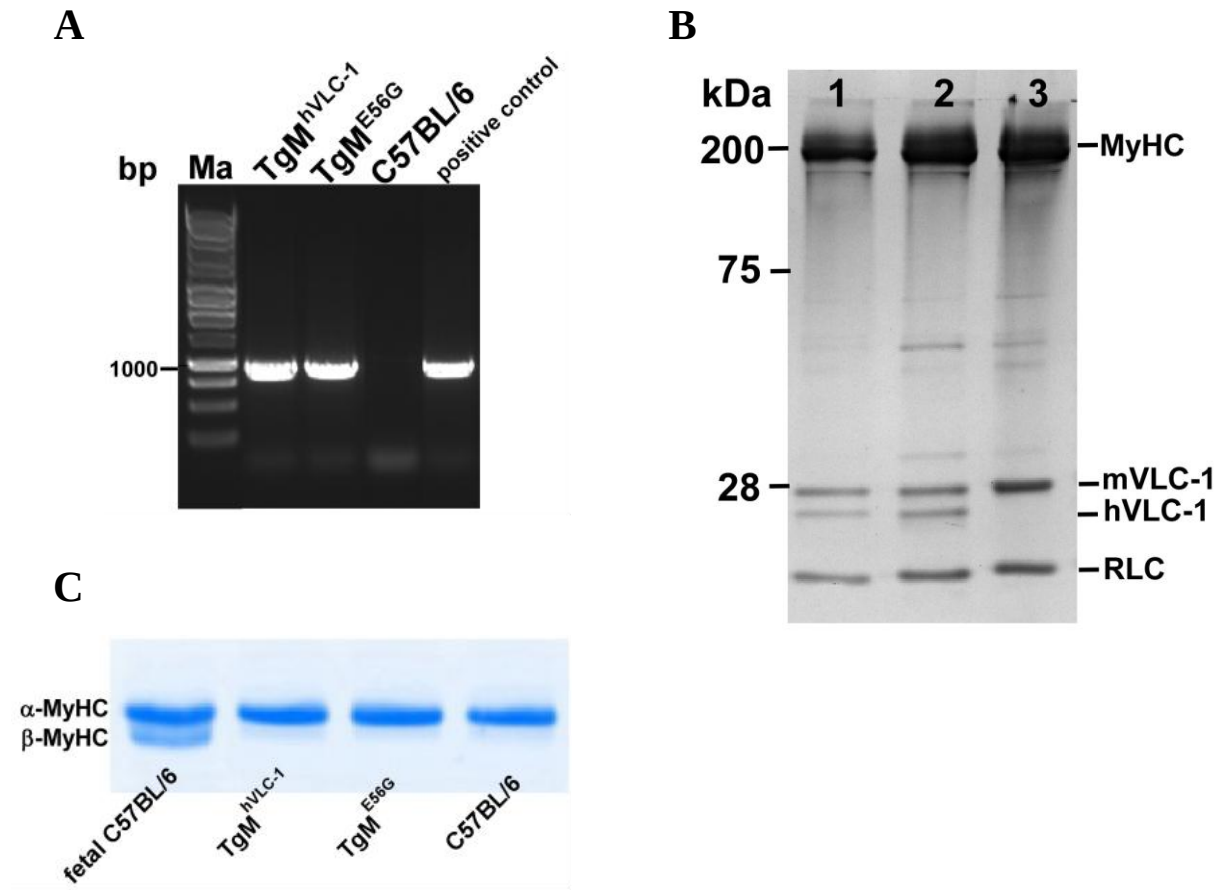
A
bp
Ma
TgM hVLC-1
TgM E56G
C57BL/6
positive control
1000
B
kDa
1
2
3
200
75
28
MyHC
mVLC-1
hVLC-1
RLC
C
α-MyHC
β-MyHC
fetal C57BL/6
TgM hVLC-1
TgM E56G
C57BL/6

Figure 2

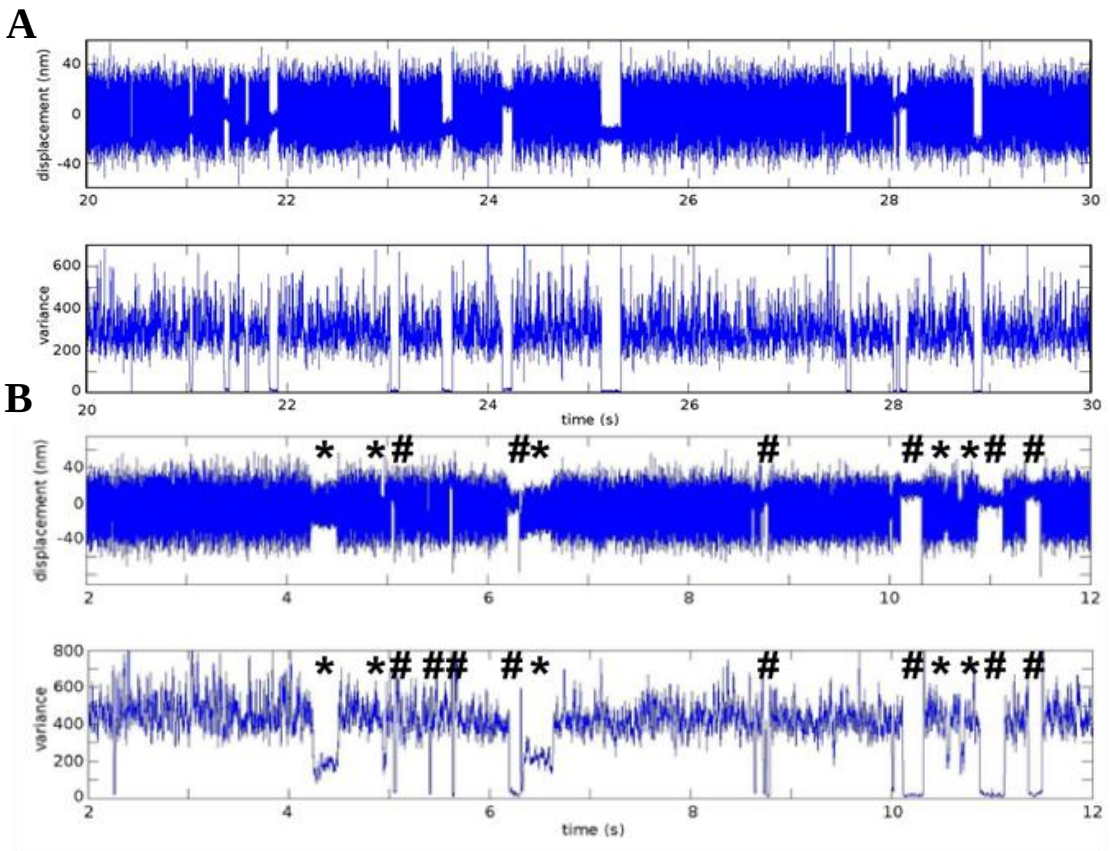
A
displacement (nm)
40
0
-40
20
22
24
26
28
30
variance
600
400
200
0
time (s)
B
displacement (nm)
* *# #* # #**# #
2
4
6
8
10
12
variance
800
600
400
200
0
* *# ## #* # #**# #
time (s)

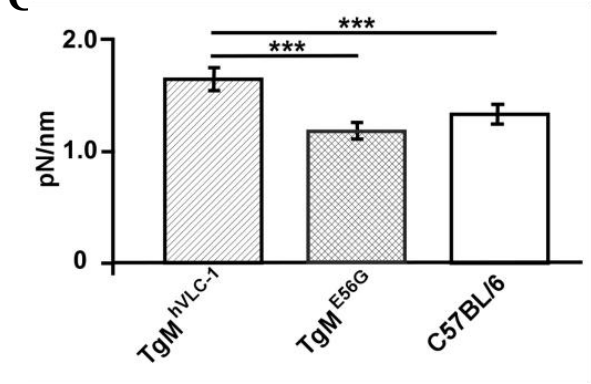
C
***
***
2.0
1.0
0
pN/nm
TgM hVLC-1
TgM E56G
C57BL/6

Figure 3

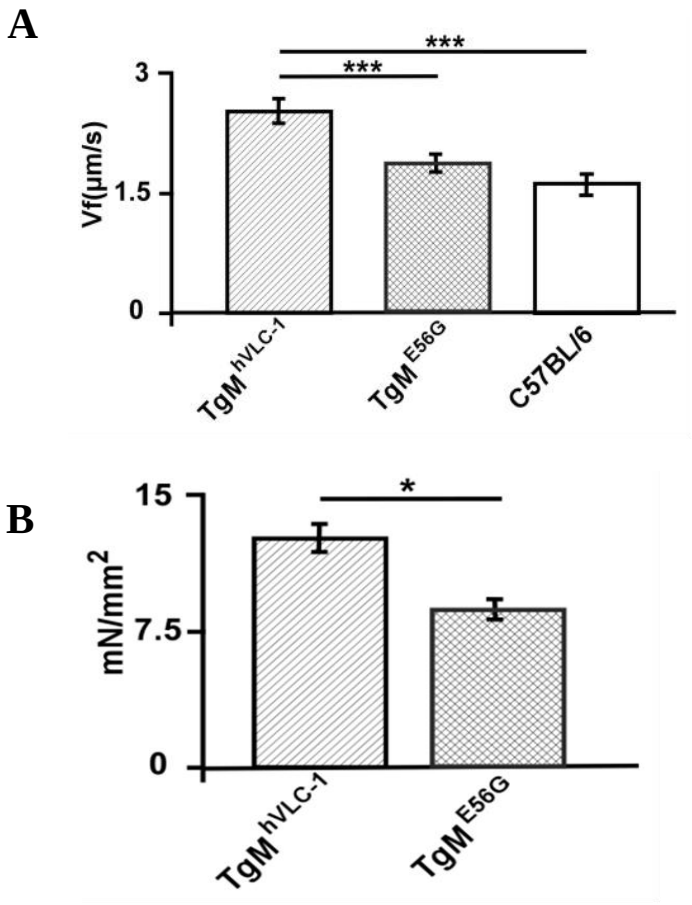
A
***
***
3
1.5
0
Vf(μm/s)
TgM hVLC-1
TgM E56G
C57BL/6
B
*
15
7.5
0
mN/mm2
TgM hVLC-1
TgM E56G

Figure 4

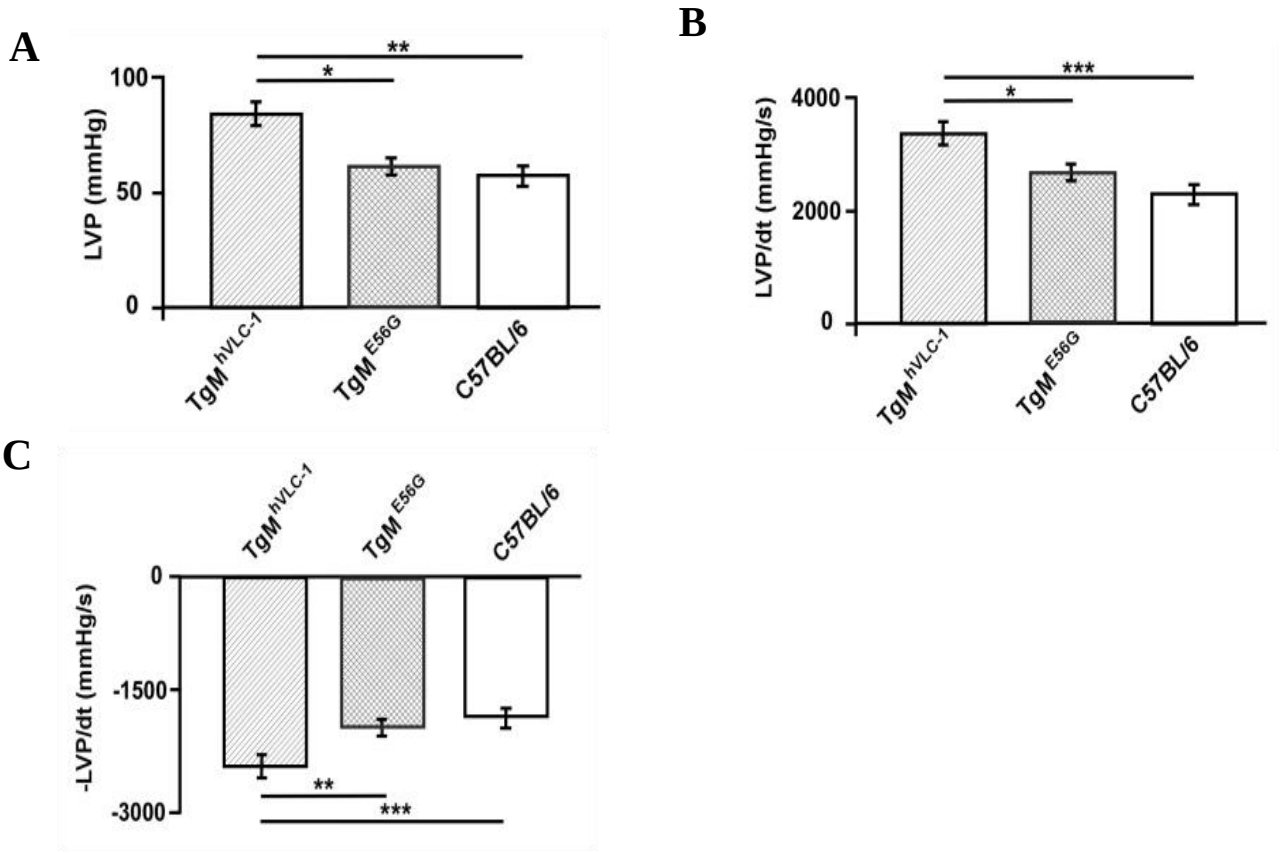
A
B
C
LVP (mmHg)
100
50
0
*
**
TgM hVLC-1
TgM E56G
C57BL/6
LVP/dt (mmHg/s)
4000
2000
0
*
***
-LVP/dt (mmHg/s)
0
-1500
-3000
**
***

Highlights

E56G-mutated essential myosin light chains (VLC-1^{E56G}) bind weakly to the myosin lever arm.
Binding of VLC-1^{E56G} to myosin reduced myosin stiffness and and actin sliding velocity.
Reduced myosin functions decreased force generation of cardiac preparations *in vitro*.
This could represent a molecular mechanism of the pathogenesis of hypertrophic cardiomyopathy.

Legend to Graphical abstract

Ventricular myosin-S1 (left) consists of a myosin heavy chain (MyHC, light blue) forming the globular motor domain and the a-helical lever arm, which is non-covalently associated with the human ventricular myosin light chain 1(hVLC-1; dark blue) and a regulatory myosin light chain (RLC, turqouis).Single ventricular myosin molecules showed high stiffness and force generating capacity. Introduction of the E56G mutation into the hVLC-12 (right; hVLC-1^{E56G}) associated with familial hypertrophic cardiomyopathy significantly reduced force myosin stiffness and force generation.

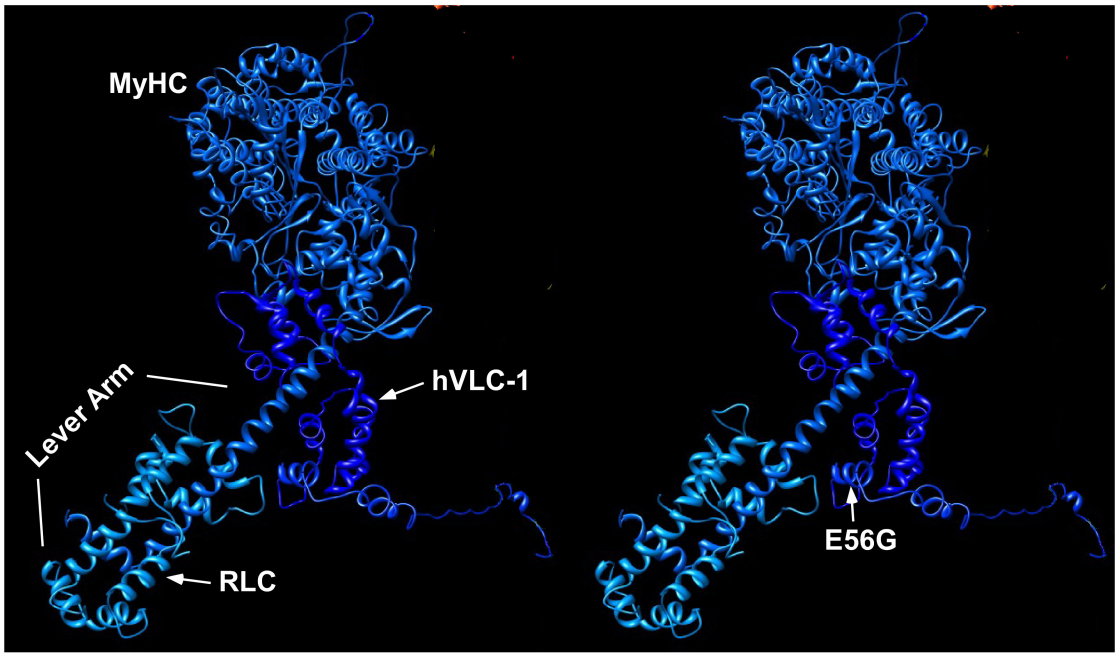

Myosin-hVLC-1
high stiffness
high force generation

Myosin-hVLC-1^{E56G}
low stiffness
low force generation

Supplementary data

Molecular mechanism regulating myosin and cardiac functions by ELC

[1]Janine Lossie[*], [1]Clemens Köhncke[*], [2,3]Shokoufeh Mahmoodzadeh[*], [4]Walter Steffen, [5]Monica Canepari, [5]Manuela Maffei, [3]Martin Taube, [3]Oriane Larchevêque, [6]Philipp Baumert, [3]Hannelore Haase, [5,7]Roberto Bottinelli, [2]Vera Regitz-Zagrosek; [3,8]Ingo Morano

[1]University Medicine Berlin Charité, Experimental and Clinical Research Center (ECRC), Germany; [2]University Medicine Berlin, Charité, Institute of Gender in Medicine, Germany; [3]Max-Delbrueck-Center for Molecular Medicine, Berlin, Germany; [4]Medizinische Hochschule Hannover; Institut fuer Molekular- und Zellphysiologie, Germany; [5]Department of Molecular Medicine and Sport Medicine Research Center, University of Pavia, Italy; [6]Johann Wolfgang Goethe-Universitaet, Institut für Sportwissenschaften, Frankfurt/Main, Germany; [7]Fondazione Salvatore Maugeri, Scientific Institute of Pavia, Pavia, Italy; [8]University Medicine Berlin Charité.

*The first three authors contributed equally to this work

Correspondence to:

Ingo Morano,
Max-Delbrück-Center for Molecular Medicine,
Robert-Roessle-Str. 10,
13125 Berlin,
Germany,
Tel: +49 30 9406 2313,
Fax: +49 30 9406 2277,
e-Mail: imorano@mdc-berlin.de

Table of content:

I) Material and Methods

I.1. Generation of transgenic mice and genotyping

All animal experiments were approved by and conducted in accordance with the guidelines set out by the State Agency for Health and Social Affairs (LaGeSo, Berlin, Germany, G 0178/07). Mice were housed at the animal facility of the MDC with a 12 h light/dark cycle and provided food and water ad libitum. We generated transgenic mouse (TgM) models overexpressing the non-mutated human ven-tricular ELC (hVLC-1) or its E56G mutated form (hVLC-1E56G), i.e. TgMhVLC-1 and TgME56G, respectively. The hVLC-1 cDNA clone (IRAUp969E0154) was obtained from imaGenes (Berlin, Germany). A single nucleotide change producing the E56G mutation was introduced using the QuikChange II site-directed mutagenesis kit (Stratagene, Amsterdam, Netherlands). cDNA of the two hVLC-1 variants (the hVLC-1 or hVLC-1E56G cDNA (590 bp) with a 630 bp 3´ untranslated poly A region of the hGH downstream) were cloned downstream into a 5.5 kb mouse α-MyHC promoter (clone 26, generously provided by Dr. J. Robbins, Cincinnati Children's Hospital Medical Center, Cincinnati, OH, USA) by HindIII sites. The α-MyHC promoter of the mouse was used to allow cardiomyocyte-specific transgene expression. The resulting transgene constructs finally contained the heart specific mouse α-MyHC promoter, including the first two noncoding exons and part of the third, followed by a Kozak-sequence and the hVLC-1 or hVLC-1E56G cDNA (590 bp) with a 630 bp 3´ untranslated poly A region of the hGH downstream. Transgene constructs were controlled by commercial DNA sequenc-ing (Stratec, Berlin, Germany). Transgene constructs were injected into the pronucleus of fer-tilized eggs derived from C57BL/6 donor mice and implanted into pseudopregnant foster mothers. Five genotypic positive founder mice with the hVLC-1E56G (TgME56G) allele and four genotypic positive founders with the human allele of the hVLC-1 (TgMhVLC-1) were identified and each bred to C57BL/6 mice.

To identify animals harbouring the transgene, genomic DNA was prepared from ear biopsies and investigated by polymerase chain reaction (PCR). The PCR was performed using a forward primer (5'-ATCTTGGCTCTTCGTCTTC- 3') located in the α-MyHC promoter and a reverse primer (5'- GCTCAGGTGTGAACTCAAT- 3') located in the transgene coding region. PCR products were separated by agarose gel electrophoresis (0.8% gel) and led to a predicted product size of 989 bp for hVLC-1 and hVLC-1E56G positive animals.

I.2. Transcriptome analysis

Three months old male transgenic mice were anaesthetized using 130 mg/kg ketamine, 20 mg/kg xylazin, and 250I.U. heparin injected i.p. Total RNA was extracted from ventricles of 3 month old male TgM^{hVLC-1} or TgM^{E56G} (four animals per group) using TRIzol reagent (Invitrogen, Life Technologies, Carlsbad, CA, USA). Total RNA was treated by Deoxyribonuclease I (TURBO DNase, Ambion) and purified using the RNeasy Purification Kit (Qiagen, GmbH, Hilden, Germany). 100 ng RNA per sample were transcribed into cDNA with Two-Cycles Target labelling and Control Reagents (Ambion WT Expression Kit and GeneChip WT Terminal Labeling and Hybridization kit, Affymetrix, Santa Clara, CA, USA). Non-pooled microarray experiments were performed with cDNA using GeneChip Mouse Gene 1.0 ST Array (28,853 genes, Affymetrix). Raw signal intensities for each probe set were analyzed using a series of methods implemented in the software package Bioconductor (http://bioconductor.org). After passing the quality control for each experiment, a set of Robust Multi-array Analysis (RMA) have been produced. The log scale RMA estimates are based upon a robust average of log2[B(PM)] (background corrected perfect match intensities).[1] To remove genes with low overall intensity or variability, normalized data were filtered by 50% intensity (selection of the genes charac-terized by having in at least 50% of the array an intensity>100). For cDNA microarrays log transformed ratios were analyzed using the Significance Analysis of Microarrays for two-class unpaired data set. For

comparison of gene lists of different experiments, genes identified by Significance Analysis of Microarrays with a False Discovery Rate (FDR) <5% and a fold-change >2 are shown.

I.3. Laser-Trap Analysis

Actin acetone powder was prepared from rabbit back muscle as described before.[2] Actin was isolated from acetone powder, purified and then biotinylated.[3] Biotinylated actin with bound rhodamine phalloidin (50 µl) was spun through 200 µl 10% sucrose (70,000g, 30 minutes) to remove monomeric actin, and resuspended with 0.1 mole Rhodamine phalloidin per mole of actin. Myosin II was isolated from mouse heart muscle as described before.[4]

Optical Trapping: The set-up was based on a Zeiss Axiovert microscope. More details are given elsewhere.[5] The positions of the two traps were controlled by electro-optical deflectors (EOD), which were used to move the 2 bead-actin filament-dumbbell relative to the myosin molecule. In order to allow relatively high tensions to be used at low trap stiffness, we used positive feedback from the quadrant detector to the EODs controlling the trap position.[6] The stiffness of the traps was determined from the relaxation time of bead position during application of square waves to the traps using the EODs. Trap stiffness was also measured from the Brownian noise of the experimental traces when the actin was not bound to myosin. The bandwidth of the 4-quadrant photo detectors was 35 kHz. Signals were sampled at 10 kHz and filtered at 5 kHz. The optical trap was calibrated as described previously.[7] In some experiments, we applied a 500 Hz sinusoidal wave to one of the beads of the dumbbell allowing for an easier detection of binding events with high compliance.[8]

Dumbbell Assay. Glass microspheres (1.5 µm) suspended in 0.075% nitrocellulose in amyl acetate were applied to 18 mm square cover slips. These were attached to slides with Tesa fotostrip (spacing ~5 mm). To ensure actin-myosin interactions were from a single molecule, the microscopic flow chambers were sparsely coated with myosin (incubation for 1 minute with 1-2 µg/ml myosin in high salt buffer, 25mM HEPES, 4mM MgCl2, 500mM KCl, 2mM

DTT, pH 7.4) such that events were found only on one out of 3-5 glass beads. The flow cell was then blocked with 1mg/ml BSA for 1 minute and a mixture of 0.8 µm neutravidin coated polystyrene beads and 1-2 nM biotinylated, Rhodamine-labeled actin was added. Reaction conditions were 5µM ATP, 4mM $MgCl_2$, 25mM KCl, 25mM Hepes, pH 7.4 and a deoxygenating system (10mg/ml glucose, 15U/ml glucose oxidase, 30µg/ml catalase). Dumbbells were assembled by attaching an actin filament to two 0.8 µm beads. The actin was stretched taught and presented over a myosin molecule bound to a 1.5 µm glass bead attached to a microscope cover slip.[9] Dumbbells were selected for low-compliance links between beads and filament such that the ratio of the position variance during free and bound periods was around 10 and above.[10] Actomyosin binding events were detected using the variance-Hidden Markov procedure[10], which also gave estimates of the stiffness of each actin-bead linkage and the myosin head. The stiffness of the links was very non-linear and a minimum tension, typically 10 pN, was required for significant noise reduction during myosin binding. To achieve relatively high link stiffness between latex beads and actin filament we stretched the dumbbell by moving the trapped beads apart at a laser power giving a trap stiffness of about 0.1 pN/nm. The total stiffness along the x-axis of the free dumbbell was then reduced by using a positive feedback system in AC mode as previously described.[6] In some experiments, we also applied a sinosoidal wave (500 Hz, 50nm peak to peak) to one side of the dumbbell which allowed an easier detection of the weak binding of myosin.

II) Tables

Table 1: Morphology and echocardiography of three months old males TgM^{hVLC-1}, TgME56G and C57BL/6.

	C57BL/6	**TgM^{hVLC-1}**	**TgM^{E56G}**
BW (g)	28.19 ± 0.61	25.9 ± 0.74	28.14 ± 0.59
LVmass (mg)	122.43 ± 5.88	120.8 ± 4.36	121.12 ± 5.0
LVmass/BW	4.33 ± 0.14	4.7 ± 0.14	4.29 ± 0.13
RWT	0.35 ± 0.01	0.35 ± 0.02	0.36 ± 0.02
HR (bpm)	426.55 ± 16.4	453.25 ± 13.6	482.50 ± 16.5
IVSd (mm)	0.75 ± 0.02	0.73 ± 0.02	0.73 ± 0.02
IVSs (mm)	1.10 ± 0.04	1.04 ± 0.04	1.13 ± 0.04
LVPWd (mm)	0.75 ± 0.02	0.73 ± 0.02	0.73 ± 0.02
LVPWs (mm)	1.07 ± 0.04	1.05 ± 0.05	1,09 ± 0.03
LVIDd (mm)	4.31 ± 0.09	4.38 ± 0.05	4.37 ± 0,1
LVIDs (mm)	3.18 ± 0.09	3.27 ± 0.08	3.09 ± 0.12
SV (µl)	32.7 ± 1.33	29.9 ± 1.73	35.5 ± 2.08
FS (%)	26.4 ± 1.05	25.5 ± 1.52	29.6 ± 1.44
EF (%)	52.2 ± 1.7	55.5 ± 2.4	54.8 ± 2.04
N	11	15	14

Bodyweight (BW), left ventricle mass (LVmass), relative wall thickness (RWT; [(IVSd+LVPWd)/LVIDd]), heart rate (HR) in beats per minute (bpm), interventricular septum thickness during diastole (IVSd) and systole (IVSs), left ventricle posterior wall thickness during diastole and systole (LVPWd, LVPWs, respectively), left ventricular internal diameter during diastole and systole (LVIDd, LVIDs, respectively), SV (stroke volume), FS (fractional

shortening), EF (ejection fraction) of 3 months old male TgMhVLC-1, TgME56G, or C57BL/6 mice. Values are expressed as means ± SEM. N = number of animals investigated.

Table 2: Microarray analysis (Affymetrix) of differentially expressed genes in TgM^{E56G} (n=4) or TgM^{hVLC-1} (n=4). FDR: False Discovery Rate. A fold-change < 0 means that the gene is down regulated in TgM^{E56G} compared to TgM^{hVLC-1}.

Gene Symbol	Description	FDR	Fold Change
U5	U5 spliceosomal RNA	0,046694	-4,33572
Uprt	uracil phosphoribosyltransferase (FUR1) homolog	0,0361973	-3,32899
Uprt	uracil phosphoribosyltransferase (FUR1) homolog	0,0407105	-2,77093
2410024N13Rik	RIKEN cDNA 2410024N13 gene	0,039736	-2,73971
2210407C18Rik	RIKEN cDNA 2210407C18 gene	0,0143476	-2,67208
Mir22hg	Mir22 host gene (non-protein coding)	0,0144842	-2,3936
Mpdz	multiple PDZ domain protein	0,00657453	-2,38032
Slc31a2	solute carrier family 31, member 2	0,035194	-2,34809
Sike1	suppressor of IKBKE 1	0,031291	-2,26305
Acot2	acyl-CoA thioesterase 2	0,0338651	-2,15197
Snx12	sorting nexin 12	0,0375959	-2,12907
SNORD50	Small nucleolar RNA SNORD50	0,0113246	-2,10452
Il2rg	interleukin 2 receptor, gamma chain	0,0317988	-2,09221
Snora34	small nucleolar RNA, H/ACA box 34	0,0428091	-2,09132
Nudt22	nucleoside diphosphate linked moiety X-type motif 22	0,0450101	-2,03719
Sly	Sycp3 like Y-linked	0,0107666	2,41232
Iqgap2	IQ motif containing GTPase activating protein 2	0,0276604	2,72585
Sly	Sycp3 like Y-linked	0,0255466	2,76581
Gm9789	predicted gene 9789	0,0497478	2,82639
E330014E10Rik	RIKEN cDNA E330014E10 gene	0,0457196	3,3962
Srsy	serine-rich, secreted, Y-linked	0,0216916	4,3202
Srsy	serine-rich, secreted, Y-linked	0,0367881	4,47968
Speer4d	spermatogenesis associated glutamate (E)-rich protein 4d	0,0384464	4,57186
Gm10722	predicted gene 10722	0,0493894	5,37452
SNORD115	Small nucleolar RNA SNORD115	0,0474845	8,04517
Ssty2	spermiogenesis specific transcript	0,00911056	8,18771
Sly	Sycp3 like Y-linked	0,0362431	9,56756
Gm10716	predicted gene 10716	0,0429258	10,3715
SNORD115	Small nucleolar RNA SNORD115	0,0360559	12,5072
LOC382133	Ssty1 family member	0,00649441	13,0578
Srsy	serine-rich, secreted, Y-linked	0,0259107	16,8086
Vmn1r-ps79	vomeronasal 1 receptor, pseudogene 79	0,02185	26,0049

III) References

[1] R.A. Irizarry, B.M. Bolstad, F. Collin, et al., Summaries of Affymetrix GeneChip probe level data, Nucleic Acids Res 31 (2003) e15.

[2] J.A. Spudich, S. Watt, The regulation of rabbit skeletal muscle contraction. I. Biochemical studies of the interaction of the tropomyosin-troponin complex with actin and the proteolytic fragments of myosin, J Biol Chem 246 (1971) 4866-4871.

[3] A. Ishijima, H. Kojima, T. Funatsu, et al., Simultaneous observation of individual ATPase and mechanical events by a single myosin molecule during interaction with actin, Cell 92 (1998) 161-171.

[4] M.J. Tyska, E. Hayes, M. Giewat, et al., Single-molecule mechanics of R403Q cardiac myosin isolated from the mouse model of familial hypertrophic cardiomyopathy, Circ Res 86 (2000) 737-744.

[5] A. Lewalle, W. Steffen, O. Stevenson, et al., Single-molecule measurement of the stiffness of the rigor myosin head, Biophys J 94 (2008) 2160-2169.

[6] W. Steffen, D. Smith, R. Simmons, et al., Mapping the actin filament with myosin, Proc Natl Acad Sci U S A 98 (2001) 14949-14954.

[7] W. Steffen, D. Smith, J. Sleep, The working stroke upon myosin-nucleotide complexes binding to actin, Proc Natl Acad Sci U S A 100 (2003) 6434-6439.

[8] C. Veigel, M.L. Bartoo, D.C. White, et al., The stiffness of rabbit skeletal actomyosin cross-bridges determined with an optical tweezers transducer, Biophys J 75 (1998) 1424-1438.

[9] J.T. Finer, R.M. Simmons, J.A. Spudich, Single myosin molecule mechanics: piconewton forces and nanometre steps, Nature 368 (1994) 113-119.

[10] D.A. Smith, W. Steffen, R.M. Simmons, et al., Hidden-Markov methods for the analysis of single-molecule actomyosin displacement data: the variance-Hidden-Markov method, Biophys J 81 (2001) 2795-2816.